State Estimation for a Legged Robot With Multiple Flexibilities Using IMUs: A Kinematic Approach

Matthieu Vigne, Antonio El Khoury, Florent Di Meglio, and Nicolas Petit

***Abstract*—This letter presents a general state estimation method for legged robots having internal flexibilities. In details, the method is applicable to any robot with an arbitrary number of punctual deformations, during standing and walking phases on flat ground. Focused on balance applications, this estimator reconstructs the position relative to the contact foot, the absolute orientation and the world velocity of each robot body. It reconciles the rigid kinematics, given by joint encoders, with attitude measurements obtained from several IMUs, through a kinematic model incorporating the flexibilities. Compared to previous works, no dynamic model of the flexibilities is employed. For illustration, the estimator is successfully tested on the exoskeleton Atalante, both in static and while walking. It is then used in closed-loop to control the position of the flying foot during a quasi-static step.**

***Index Terms*—Legged robots, prosthetics and exoskeletons, humanoid and bipedal locomotion, sensor fusion.**

I. Introduction

TO REALIZE complex tasks such as balancing or walking, a legged robot requires an accurate state estimation [1], i.e. knowledge of the position and velocities of the robot bodies relative to an inertial frame. For instance, the position of the center of mass is a required variable to determine whether the system is statically balanced. Likewise, walking gaits are usually executed by estimating and controlling the center of pressure [2].

For a fully rigid robot, with known kinematics and equipped with joint encoders, the six degrees of freedom defining the pose of the floating base remain unmeasured. These degrees of freedom are classically estimated by integrating data from an inertial measurement unit (IMU) and fusing it with contact information coupled with the robot kinematics. To cite a few examples, in [3] and [4], this fusion is performed thanks to an Extended Kalman Filter, using for process model a simple integration of IMU data - binary contact information and rigid kinematics provide a measurement for the position of the IMU.

Manuscript received June 3, 2019; accepted October 22, 2019. Date of publication November 11, 2019; date of current version November 29, 2019. This letter was recommended for publication by Associate Editor A. Jafari and Editor N. Tsagarakis upon evaluation of the reviewers' comments. *(Corresponding author: Matthieu Vigne.)*

M. Vigne is with Wandercraft, 75004 Paris, France, and also with Centre Automatique et Systèmes, MINES ParisTech, PSL, 75006 Paris, France (e-mail: matthieu.vigne@wandercraft.eu).

A. El Khoury is with Wandercraft, 75004 Paris, France (e-mail: antonio.elkhoury@wandercraft.eu).

F. Di Meglio and N. Petit are with Centre Automatique et Systèmes, MINES ParisTech, PSL, 75006 Paris, France (e-mail: florent.di_meglio@mines-paristech.fr; petit@cas.ensmp.fr).

Digital Object Identifier 10.1109/LRA.2019.2953006

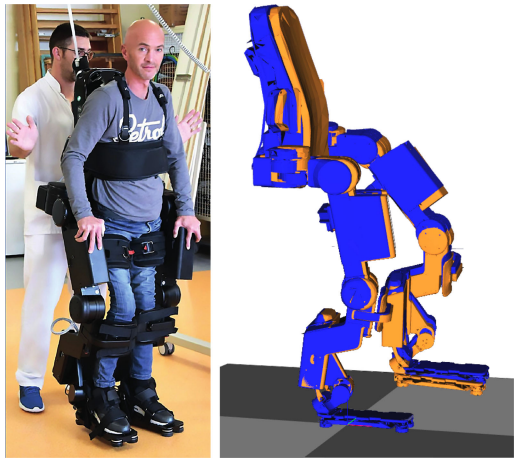

Fig. 1. Picture of the exoskeleton Atalante. On the right, CAD reconstruction under the assumption of full rigidity (blue), and ground truth from motion capture (orange).

This idea is further developed in [5], where the contact body orientation is also constrained (as is the case for a humanoid with flat foot). In [6] a similar observer is presented, using an Invariant Kalman filter.

By contrast, the problem becomes more complex if, instead of considering a rigid structure, the robot has internal flexibilities. This is often the case for humanoid robots, as a result of design constraints, or a voluntary choice, as compliance protects the structure from hard impacts. This is for instance the case of Atalante [7], an exoskeleton developed by Wandercraft, serving as illustration in the article (see Fig. 1). Due to these flexibilities, it is not enough to rely on the rigid kinematics of the robot to get full state information, as they introduce new degrees of freedom. For this reason, the previous approaches cannot be applied as-is. Assuming that the robot is anchored to the ground (to remove floating base estimation), IMUs have been used to estimate the state of the flexibility. The authors of [8] model a flexibility at the robot ankle as extra degrees of freedom into a kinematic chain, whose state is estimated and then re-injected into the extended kinematics; a similar approach is taken in [9]. A dynamic model of the flexibilities can also be considered as in [10]. The use of such a model could enable the design of dynamics-based observers such as done in rigid robots in [11] or [12] for instance. In our previous work [13], we extended the framework of [10] to the presence of several punctual flexibilities, dynamically modeled as springs in an Extended Kalman Filter. This observer, however, requires an accurate dynamic model (i.e. accurate

values of flexibility stiffness, link inertia...) which is not easy to obtain, in particular for an exoskeleton working with a human.

In this letter, we tackle the novel problem of state estimation for a legged robot with multiple punctual flexibilities, both when standing and when walking on flat ground (a suitable hypothesis for an indoor exoskeleton such as Atalante). The main contribution is a state-estimation methodology, that relies on decomposing the full estimation problem into several independent attitude estimation problems, each corresponding to a given flexibility and a given IMU. An important property is that this approach only relies on dependable and easily accessible geometric parameters of the system, and not on the dynamic model, which is highly uncertain on an exoskeleton due to the presence of an uninstrumented moving human.

Experimental results illustrate the effectiveness of this method, which outperforms our previously proposed dynamics-based approach. This estimator is subsequently used for closed-loop control, to compensate for the effect of these deformations.

The paper is organized as follows: in Section II we define a kinematic model to represent the flexible structure. In Section III, we expose our estimation method. Section IV reports experimental results obtained on the robotic platform, both in open-loop (to validate the estimator) and in closed-loop, where a simple control strategy is used based on the proposed estimator.

II. System Modeling

A. Problem Statement

The exoskeleton Atalante, under study here, exhibits a flexible behavior, as can be seen in Fig. 1. Indeed, when placed on the ground in single support, the real position of the robot links (in orange, as seen by a motion capture device) does not match the expected rigid position (in blue), generated by the kinematic model and joint encoders: there is a mismatch of about 4 cm in the position of the flying foot. This error is detrimental to system performance: for instance, instead of walking smoothly, the exoskeleton tends to stumble forward as the foot strikes the ground too early. The aim of this letter is to estimate this difference, in other words, to estimate the relative position and velocity of the robot links, generated by the flexibilities.

More formally, we consider a legged robot with flat feet, standing or walking on the ground. We make the following assumption:

Assumption 1: At any given time, there is at least one foot in flat contact with the ground.

We assume knowledge of the contact foot, through, for instance, contact or force sensor on the robot, something quite common for a walking system. This assumption enables us to easily define the floating base classically used to define the coordinates of a mobile robot, turning the system into a kinematic tree with a fixed base. Specifically, we call W the fixed inertial frame of reference, and define $\mathcal{L}$ the local frame centered at the contact foot, rotated from the world frame by a rotation around the vertical axis $\boldsymbol{e}_z$ to remain aligned with the foot. Then, assuming the robot to be fully rigid, the state of the robot in the local frame is entirely determined by the joint configuration, $\boldsymbol{q}$ and $\dot{\boldsymbol{q}}$, which are measured using joint encoders and relevant numerical derivatives.

However, full rigidity is, for many systems including Atalante, an unrealistic assumption. Indeed, punctual deformations are often present, in particular at or around the robot joints, which represent weaker points in the structure. Unlike joints of the rigid model, these flexibilities cannot be easily instrumented by joint encoders. They introduce extra degrees of freedom to the system. In this study, we consider n punctual deformations, distributed throughout the structure. The problem under consideration in this letter can thus be formulated as follows

Problem 1: Under Assumption 1, estimate the local position and orientation ${}^{\mathcal{L}}M_{\mathcal{B}}$ and the velocity with respect to the world inertial frame, expressed in the local frame, ${}^{\mathcal{L}}\boldsymbol{v}_{\mathcal{B}/W}$, of every body $\mathcal{B}$ of the robot.

B. Kinematic Model of the Flexibilities

In the absence of flexibilities, the rigid kinematics of the robot relates the pose ${}^{\mathcal{L}}M_{\mathcal{B},r}$ of any body $\mathcal{B}$ in the local frame to the joint encoders readings $\boldsymbol{q}$ according to

$$\begin{cases} {}^{\mathcal{L}}M_{\mathcal{B},r} = f_r(\boldsymbol{q}) \\ {}^{\mathcal{L}}\boldsymbol{v}_{\mathcal{B}/W,r} = J_r(\boldsymbol{q})\dot{\boldsymbol{q}} \end{cases} \tag{1}$$

where f_r represents the rigid kinematics and J_r its Jacobian. Thus, ${}^{\mathcal{L}}M_{\mathcal{B},r}$ is the best position estimate we can make using only encoders information. Note that f_r depends on the contact foot - for simplicity of notation this dependency is omitted here.

We make the following assumption to represent the punctual deformations under study here:

Assumption 2: Each flexibility corresponds to a rotation about a known point O_i, $i = 1, \ldots, n$.

For each point O_i, we call D_i the rotation matrix representing all the deformations taking place in the system up to O_i. Then, D_i is defined as

$$D_i \triangleq {}^{\mathcal{L}}R_{\mathcal{B}_i}\,{}^{\mathcal{L}}R^T_{\mathcal{B}_i,r} \tag{2}$$

for $\mathcal{B}_i$ a body located after O_i in the kinematic tree, and before the next flexibility. ${}^{\mathcal{L}}R^T_{\mathcal{B}_i,r}$, the rigid configuration of $\mathcal{B}_i$, is computed according to (1). In other words, D_i is the rotation taking the body from its rigid position to its real orientation. Fig. 2 pictures how these deformations alter the geometry of the system.

An important consequence of Assumption 2 is that the flexible system still forms a kinematic tree, with coordinates $(\boldsymbol{q}, D_1, \ldots, D_n)$. Thus, the state of any rigid body $\mathcal{B}$ of this system can be written as a function of these variables only, according to

$$\begin{cases} {}^{\mathcal{L}}M_{\mathcal{B}} = f_f(\boldsymbol{q}, D_1, \ldots, D_n) \\ {}^{\mathcal{L}}\boldsymbol{v}_{\mathcal{B}/W} = J_f(\boldsymbol{q}, D_1, \ldots, D_n) \begin{pmatrix} \dot{\boldsymbol{q}} \\ \boldsymbol{\omega}_1 \\ \ldots \\ \boldsymbol{\omega}_n \end{pmatrix} \end{cases} \tag{3}$$

with $\boldsymbol{\omega}_i$ the angular velocity associated to D_i in frame $\mathcal{L}$, and f_f, J_f, the corresponding kinematic model and Jacobian.

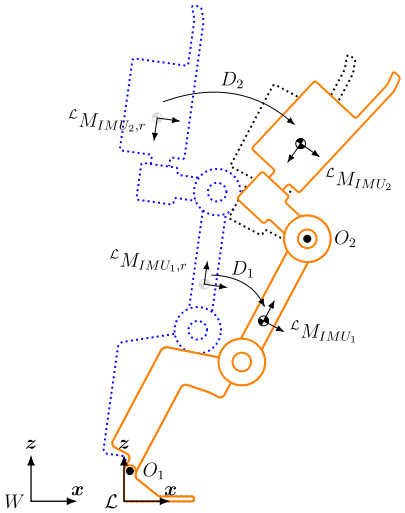

Fig. 2. Representation of the flexible model: the blue dotted configuration corresponds to the rigid system f_r, the orange gives the flexible kinematics f_f.

III. Estimator Design

Equation (3) gives a natural way of obtaining a position and velocity estimation for any body $\mathcal{B}$ of the flexible system. Indeed, if for all $i = 1 \dots n$, an estimate $\hat{D}_i$ of the deformations, and an estimate $\hat{\boldsymbol{\omega}}_i$ of the velocity are available, then the kinematic model (3) gives an estimate for $\mathcal{B}$ as

$$\begin{cases} {}^{\mathcal{L}}\hat{M}_{\mathcal{B}} = f_f(\boldsymbol{q}, \hat{D}_1, \dots, \hat{D}_n) \\ {}^{\mathcal{L}}\hat{\boldsymbol{v}}_{\mathcal{B}/W} = J_f(\boldsymbol{q}, \hat{D}_1, \dots, \hat{D}_n) \begin{pmatrix} \dot{\boldsymbol{q}} \\ \hat{\boldsymbol{\omega}}_1 \\ \dots \\ \hat{\boldsymbol{\omega}}_n \end{pmatrix} \end{cases} \tag{4}$$

Thus, the state estimation problem boils down to n independent attitude estimation problems. A common solution for each attitude estimation is to use IMU sensors, composed of a triaxial accelerometer and triaxial gyroscope (see for instance [14]–[16]). These sensors have many technological advantages: they are affordable, lightweight and straightforward to integrate into a mechanical system. These properties are important given that we need to use several of these sensors to estimate the multiple flexibilities of the structure. Indeed, we place n IMUs on the system, one after each deformation along the kinematic tree. Thus, the attitude of IMU_i is related to D_i according to (2) applied to $\mathcal{B} = IMU_i$:

$${}^{\mathcal{L}}R_{IMU_i} = D_i {}^{\mathcal{L}}R_{IMU_i,r} \tag{5}$$

This equation enables us to partially reconstruct the deformation D_i (as only part of the IMU attitude is observable, see Section III-A). Meanwhile, the strapdown gyroscope gives a direct measurement of the body angular velocity, from which we compute the deformation velocity $\boldsymbol{\omega}_i$ (see Section III-B). Gathering all the ingredients sketched above, we can now formulate the following algorithm which builds an estimator based on (3) to solve Problem 1:

- **Step 1:** Using contact sensor information, determine the current ground contact point: this indicates the flexible model f_f to use.
- **Step 2:** Using encoder information, determine the attitude of each IMU ${}^{\mathcal{L}}R_{IMU_i,r}$ in the absence of deformation.
- **Step 3:** Estimate the attitude of each IMU using sensor data. Comparing this with the rigid orientation, compute a (partial) estimate of the deformation matrix $\hat{D}_i$: this is detailed in Section III-A, (18).
- **Step 4:** Using the previously estimated attitude, express the gyroscope readings $\boldsymbol{y}_{g_i}$ in the appropriate frame to get an estimate of $\boldsymbol{\omega}_i$: this is detailed in Section III-B, (22).
- **Step 5:** Using the estimates defined above, apply (4) to any body of the system to compute its state.

We believe that a strength of the proposed methodology is to rely on several simple steps, giving a modular approach. Indeed, the kinematic models f_r and f_f are both kinematic trees, and can thus be computed using well-known algorithms like the ones described in [17]: the implementation used for this letter relies on the open-source library *Pinocchio* [18]. Thus, Step 1, 2, 4 and 5 carry no practical implementation difficulty. The only true observation step is done in Step 3, where we estimate an attitude from IMU measurements: this is a classical problem well tackled by state-of-the-art observers, which we discuss in Section III-A. Thus, our estimation method consists only in taking a state-of-the-art observer and injecting it into this readily-available model.

In the next two subsections, we will detail respectively Steps 3 and 4, i.e we will show how to use IMU data to acquire an estimate of the deformation and its angular velocity.

A. Deformation Estimation

For the sake of completeness, we first briefly recall how a strapdown IMU can be used to compute a partial attitude estimation, ${}^{\mathcal{L}}\hat{R}_{IMU}$, which we will use to reconstruct the deformation rotation $\hat{D}_i$. The IMU measurements write

$$\begin{cases} \boldsymbol{y}_a = {}^{\mathcal{L}}R_{IMU_i}^T(\boldsymbol{a} - \boldsymbol{g}) + \boldsymbol{\nu} & (6) \\ \boldsymbol{y}_g = {}^{\mathcal{L}}R_{IMU_i}^T {}^{\mathcal{L}}\boldsymbol{\omega}_{IMU/W} + \boldsymbol{b}_g + \boldsymbol{\mu} & (7) \end{cases}$$

with $\boldsymbol{a}$ the sensor linear acceleration with respect to the world frame, expressed in the local frame, $\boldsymbol{g}$ gravity, $\boldsymbol{b}_g$ an additive gyro bias (we neglect accelerometer bias before $\boldsymbol{g}$), ${}^{\mathcal{L}}\boldsymbol{\omega}_{IMU/W}$ the sensor angular velocity with respect to the world frame in the local frame, and $\boldsymbol{\nu}$, $\boldsymbol{\mu}$ (supposedly) Gaussian white noises.

We here make the classical assumption that the sensor acceleration is, on average, negligible compared to gravity [14]: indeed it is quite clear for any human that, while walking, gravity remains the dominant force. As will appear in Section IV, this assumption is valid even during walking experiments. Thus, the deterministic accelerometer output writes

$$\boldsymbol{y}_a = -{}^{\mathcal{L}}R_{IMU_i}^T \boldsymbol{g} \tag{8}$$

Eq. (8) stresses that a rotation around the gravity vector leaves the sensor output unchanged: hence, this component of rotation is unobservable with such sensors. This is a well-known result, [14], which can be formulated using the notion of tilt [15]:

Definition 1: Let $\boldsymbol{e}_z$ be the world frame vertical axis. For any rotation $R \in SO(3)$, we call *tilt* the vector

$$\boldsymbol{t}(R) = R^T \boldsymbol{e}_z \tag{9}$$

According to (8), the IMU sensor thus provides only an estimate of the tilt $\boldsymbol{t}({}^{\mathcal{L}}R_{IMU})$. There exist many observers to reconstruct this tilt estimation: for the experimental results shown here, we use the nonlinear observer designed in [14, Equation (48)]. This filter estimates both the attitude of the IMU, ${}^{\mathcal{L}}R_{IMU_i}$, and the gyroscope bias, $\boldsymbol{b}_g$, modeled as a constant, as follows

$$\begin{cases} \boldsymbol{\omega} = \boldsymbol{y}_a \times {}^{\mathcal{L}}\hat{R}^T_{IMU_i}\boldsymbol{g} \\ {}^{\mathcal{L}}\dot{\hat{R}}_{IMU_i} = {}^{\mathcal{L}}\hat{R}_{IMU_i}\left[\boldsymbol{y}_g - \hat{\boldsymbol{b}}_g + k_p\boldsymbol{\omega}\right]_\times \\ \dot{\hat{\boldsymbol{b}}}_g = -k_I\boldsymbol{\omega} \end{cases} \tag{10}$$

where $[\boldsymbol{v}]_\times$ is the skew-symmetric matrix associated to the vector $\boldsymbol{v}$, k_p and k_I are positive observer gains. This observer is proven in [14] to be globally convergent, provided some persistent excitation condition is satisfied, except on an unstable zero-measure subset; it has the advantage of being simple to implement and tune, when compared for instance to a state-of-the-art Extended Kalman Filter.

Using (5), we interpret the attitude estimation given by the complementary filter as a deformation of the rigid structure:

$$\widetilde{D}_i \triangleq {}^{\mathcal{L}}\hat{R}_{IMU_i}\,{}^{\mathcal{L}}R^T_{IMU,r} \tag{11}$$

However, only the tilt of ${}^{\mathcal{L}}\hat{R}_{IMU_i}$ is observable: similarly, only the tilt of $\widetilde{D}_i$ is relevant, as

$$\boldsymbol{t}(\widetilde{D}_i) = {}^{\mathcal{L}}R_{IMU,r}\,{}^{\mathcal{L}}\hat{R}^T_{IMU_i}\boldsymbol{e}_z = {}^{\mathcal{L}}R_{IMU,r}\boldsymbol{t}({}^{\mathcal{L}}\hat{R}_{IMU_i}) \tag{12}$$

While some approaches can be used to limit the drift of the unobservable component of the rotation (see e.g. [19]), we make here a stronger reconstruction choice: the unobservable part of the rotation $\widetilde{D}_i$ is nullified (i.e. arbitrarily set to identity). This choice is motivated by the fact that $\widetilde{D}_i$ represents the deformation of the system: for a system where gravity is the dominant force, as is the case of a walking robot, the deformation around the vertical axis is expected to be small. This hypothesis could be relaxed if other measurements (for example, vision sensors) or a dynamic model of the flexibility render this component observable.

The unobservable part of the rotation $\widetilde{D}_i$ can be removed using the well-known twist-swing decomposition [20]. We here show that this decomposition is indeed well-suited to the current problem.

For two non-zero vectors $\boldsymbol{a}$, $\boldsymbol{b}$, we write $\alpha(\boldsymbol{a},\ \boldsymbol{b})$ the angle from $\boldsymbol{a}$ to $\boldsymbol{b}$. We first restate a classical result to define a norm on $SO(3)$[21]:

Definition 2: Let R in $SO(3)$; there exists a unit vector $\boldsymbol{v}$ and a scalar θ such that R is the rotation around $\boldsymbol{v}$ of angle θ. We write $R = \mathcal{R}(\boldsymbol{v}, \theta)$. This defines a norm on $SO(3)$ as: $||R|| = |\theta|$. Furthermore, this norm is characterized by

$$||R|| = \max_{\{\boldsymbol{a}\in\mathbb{R}^3 \mid ||\boldsymbol{a}||=1\}} |\alpha\left(\boldsymbol{a},\ R\boldsymbol{a}\right)| \tag{13}$$

For simplicity of notations, we extend the $\mathcal{R}$ operator to non-unit vectors as follows:

$$\forall \boldsymbol{v} \in \mathbb{R}^3, \mathcal{R}(\boldsymbol{v}, \theta) = \begin{cases} \mathcal{R}\left(\frac{\boldsymbol{v}}{||\boldsymbol{v}||}, ||\boldsymbol{v}||\theta\right) & \text{if } \boldsymbol{v} \neq 0 \\ I_3 & \text{if } \boldsymbol{v} = 0 \end{cases} \tag{14}$$

Using this norm, the twist-swing decomposition can be defined as follows:

Theorem 1: Any rotation matrix R can be decomposed as

$$R = R_z R_s \tag{15}$$

where R_z (the twist) is a rotation around $\boldsymbol{e}_z$ and R_s (the swing) is the smallest (in norm) rotation matrix such that $\boldsymbol{t}(R_s) = \boldsymbol{t}(R)$. In other words,

$$R_s = \underset{\{P\in SO(3) \mid \boldsymbol{t}(P)=\boldsymbol{t}(R)\}}{\arg\min} ||P|| \tag{16}$$

If additionally $R^T\boldsymbol{e}_z \neq -\boldsymbol{e}_z$, this decomposition is unique, and is given by the following formula:

$$R_s = \mathcal{R}\Big(\boldsymbol{e}_z \times \boldsymbol{t}(R), ||\boldsymbol{e}_z \times \boldsymbol{t}(R)||\alpha\left(\boldsymbol{e}_z,\ \boldsymbol{t}(R)\right)\Big) \tag{17}$$

For completeness, the proof of this "folk" result is given in Appendix A.

Applying (17) on $\widetilde{D}_i$ gives the desired rotation matrix $\hat{D}_i$, that is, the rotation matrix with zero non-observable component describing the tilt of the IMU:

$$\hat{D}_i \triangleq \mathcal{R}\Big(\boldsymbol{e}_z \times \boldsymbol{t}(\widetilde{D}_i), ||\boldsymbol{e}_z \times \boldsymbol{t}(\widetilde{D}_i)||\alpha\left(\boldsymbol{e}_z,\ \boldsymbol{t}(\widetilde{D}_i)\right)\Big) \tag{18}$$

Note that since $\widetilde{D}_i$ accounts for a small rotation error, the condition $\widetilde{D}_i\boldsymbol{e}_z \neq -\boldsymbol{e}_z$ required to apply (17) in Theorem 1 will always be met in practice.

B. Velocity Estimate

In this part, we derive an estimate $\hat{\boldsymbol{\omega}}_i$ of the angular velocity of the deformations from gyroscope readings.

Let ${}^{IMU_i}\boldsymbol{\omega}_{IMU_i/W,r}$ be the angular velocity of the IMU due to the rigid motion only, in the sensor frame: this quantity is a function of encoder measurements only, according to (1). Then, the angular velocity, relative to the world frame, in the local frame, is the sum of the rigid and flexible angular velocities according to

$${}^{\mathcal{L}}\boldsymbol{\omega}_{IMU_i/W} = \boldsymbol{\omega}_i + {}^{\mathcal{L}}R_{IMU_i}\,{}^{IMU_i}\boldsymbol{\omega}_{IMU_i/W,r} \tag{19}$$

Injecting (7) into (19) yields

$$\boldsymbol{\omega}_i = {}^{\mathcal{L}}R_{IMU_i}(\boldsymbol{y}_g - \boldsymbol{b}_g - \boldsymbol{\mu} - {}^{IMU_i}\boldsymbol{\omega}_{IMU_i/W,r}) \tag{20}$$

Neglecting the noise $\boldsymbol{\mu}$ and using the deformation estimates from (18) and the bias estimate from (10) yields

$$\hat{\boldsymbol{\omega}}_i = \hat{D}_i\,{}^{\mathcal{L}}R_{IMU_i,r}(\boldsymbol{y}_g - \hat{\boldsymbol{b}}_g - {}^{IMU_i}\boldsymbol{\omega}_{IMU_i/W,r}) \tag{21}$$

This equation only translates the algebraic computation needed to subtract the "rigid" velocity and the bias from the gyroscope, in order to isolate the velocity due to the flexibilities. In practice however, to attenuate the effects of the gyroscope additive noise, neglected in (21), a low-pass filter LP is first

applied to the gyroscope output, yielding

$$\hat{\boldsymbol{\omega}}_i = \hat{D}_i {}^{\mathcal{L}}R_{IMU_i,r} \left(LP(\boldsymbol{y}_g) - \hat{\boldsymbol{b}}_g - {}^{IMU_i}\boldsymbol{\omega}_{IMU_i/W,r} \right) \quad (22)$$

IV. Experimental Results

In this section, we report experimental results obtained on the exoskeleton Atalante, pictured in Fig. 1, to validate the current methodology.

This robot is equipped with force sensors, enabling us to identify at any given time the contact foot, as needed for this approach. The flexibilities are studied using a motion capture system composed of 8 infrared cameras from Optitrack to provide ground-truth information. This study establishes that, in single support, the robot deforms at three points: the support ankle, and both hips. Thus, three IMUs are placed on the system, one in each leg and one in the robot pelvis, which is consistent with our requirement of having one IMU for each deformation. Note that for simplicity, we are not considering a deformation at the flying foot ankle. Indeed, once a contact foot is defined, the robot forms an open kinematic chain, and the flying ankle is at the very end of the chain: thus, a deformation happening there impacts only the flying foot, which, in turn, has little impact on the behavior of the rest of the system. Furthermore, when this foot is airborne, there is no deformation at the ankle which supports only very little load.

In the experimental results presented thereafter, we use low-cost MEMS IMUs. Alignment biases are identified during a no-load preliminary experiment. The sensors are all sampled at 1 kHz. For angular velocity estimation, the gyroscope is filtered by a first-order low-pass with a cutoff frequency of 25 Hz: this value was empirically determined to significantly reduce the impact of noise while providing a negligible lag for the experiments of interest, i.e. cyclic walking patterns around 1 Hz. A video of all experiments is available in [22].

A. Estimator Validation

In this part, we assess the performance of the estimator both in a static case and on a dynamic walking gait, against ground truth from motion capture. This estimator is compared with the use of the rigid model only, and with the extended Kalman filter (EKF) presented in [13]. Contrary to the current approach, this EKF relies not only on the kinematics but also on the dynamics of the system, assuming that the flexibilities behave like a linear spring, whose stiffness can be identified experimentally on the system.

1) Static Experiment: This first test case is similar to the one used in [13] to validate the EKF: the empty exoskeleton is placed on the ground in single support, in a posture similar to that of Fig. 1, and is manually pushed to generate excitation of the flexibilities. Natural damping yields a slow decay of the oscillations.

Table I and Fig. 3 show a comparison of the various estimations of the flying foot and pelvis position. Despite its apparent simplicity, the proposed estimator yields a very accurate estimate, as both the pelvis and the flying foot positions are reconstructed with a root-mean-square error (RMSE) of only

TABLE I
Root Mean Square Error of Position Estimates, Static

	Flying foot RMSE (cm)			Pelvis RMSE (cm)		
	x	y	z	x	y	z
Rigid model	1.5	1.1	3.3	2.7	1.4	1.0
EKF	0.4	1.9	1.0	2.1	1.2	0.1
Proposed estimator	0.2	0.5	0.3	0.5	0.2	0.1

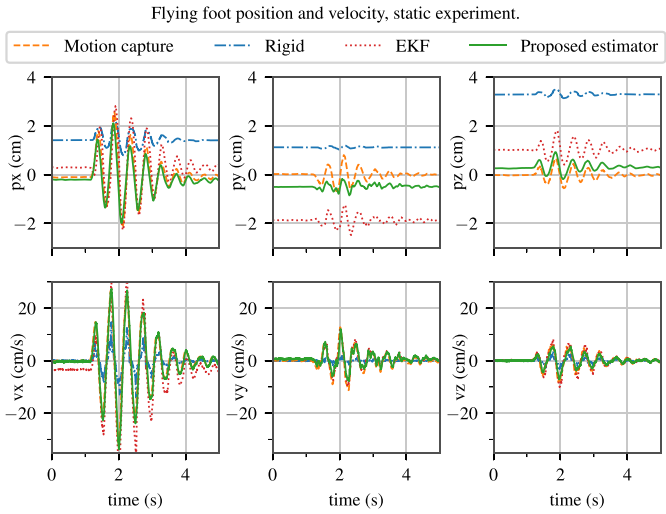

Fig. 3. Flying foot position and velocity during a single support experiment. The exoskeleton was pushed to generate excitation of the flexibilities. x is an axis pointing forward, z the upward vertical axis.

0.5 cm for each axis. It even outperforms the EKF : while both manage to capture the oscillations of the system, the EKF is characterized by a larger bias. This comes from the fact that errors in the dynamic model change the equilibrium state of the system: it now depends in particular on the stiffness parameters, which are difficult to estimate. For the EKF results presented in this letter, we use the theoretical CAD model of the exoskeleton, and experimentally identified stiffness. We do believe that a more accurate system identification and the use of advanced estimation techniques [11], [12] would improve the results of the dynamics-based observer in the context of a legged robot. However, the presence of a user in the exoskeleton makes identification of a static model impossible, since his motion radically changes the system dynamics, e.g. by displacing the center of mass in an unmeasured fashion, or creating unknown internal forces. By contrast, the proposed methodology offers a ready-to-use estimator with quite satisfactory results, at almost zero calibration cost. We further illustrate this point in the next section by performing walking experiments with a user.

2) Walking Experiment: We now consider a more realistic scenario : a walking gait with a user onboard. Walking is, arguably, a more challenging motion for our estimator, for two reasons. First, dynamic motion generate non-zero contributions to the accelerometer readings. Likewise, impacts, which cause large acceleration spikes, have the same effect: the accelerometers no longer measure gravity. However, the accelerations during walking remain small compared to gravity - and the leg

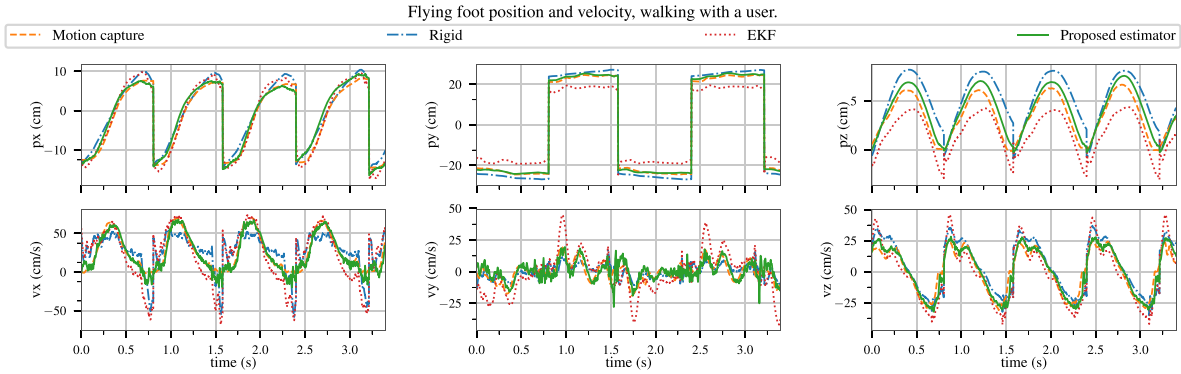

Fig. 4. Position and velocity of the flying foot during a walking gait, computed by the rigid model, the EKF from [13], our estimator, and motion capture.

IMUs, which undergo most of the acceleration, are at rest every other step. Impacts are also very brief, and thus well filtered by the observer (10), granted that mild gains are used: indeed, the average orientation error of this observer (compared to motion capture) during the walk is only $0.8°$. Thus, unlike dynamics-based observers which usually require knowledge of the impacts dynamics, modeled as a discontinuity in the velocity [11], our observer does not require specific treatment of impact.

Second, we have assumed in our estimator design that, at any given time, the stance foot is in flat contact with the ground: in practice, the stance foot is usually not perfectly flat. A reason for that is the deformations themselves: they cause the flying foot to strike the ground earlier than planned, with a non-zero angle. This causes a momentary mismatch in the model, in particular after impact, and Assumption 1 non longer holds. However, since the IMUs give a measurement of the absolute attitude of the sensor, this phenomenon is indirectly taken into account in our estimator as a deformation around the ankle. Thus, the only error is the center of rotation: we consider this rotation to be taking place at the ankle, whereas in fact is occurs at the foot edge. Since the distance between these points is rather small, and the corresponding angle remains small, the resulting error is negligible.

Note that, since having a user inside the exoskeleton does not modify the kinematics of the system, it has no direct impact on our estimator, that can be used as is, regardless of the morphology of the patient. This is not the case for the EKF, that would require not only the mass and inertia of the patient, but also the knowledge of the user motion inside the exoskeleton. Nevertheless, for the sake of comparison, we consider that the user is standing perfectly still, and used an antropometric model as found in [23] to represent the user in the EKF model.

Fig. 4 and Table II show the result of a such a walking experiment. Though the root mean square error of the proposed estimator has increased, when compared to the static case in Table I, the result remains quite satisfactory, with approximately 1 cm of error in each axis. Likewise, the velocity estimation is drastically improved, as can be seen in Fig. 4. Indeed, the rigid model gives a velocity quite far from motion capture, in particular after the impact, where we see large spikes: this comes from the fact that, right after impact, the ankle motors move to put the new stance foot horizontal on the ground - a motion captured by the encoders, but that occurs without any significant leg motion.

TABLE II
ROOT MEAN SQUARE ERROR OF POSITION ESTIMATES, WALKING

	Flying foot RMSE (cm)			Pelvis RMSE (cm)		
	x	y	z	x	y	z
Rigid model	1.6	2.6	2.3	2.6	4.3	1.0
EKF	1.9	5.0	2.1	3.5	3.1	1.4
Proposed estimator	1.1	0.7	0.9	0.6	1.1	0.5

The performance of the EKF however drastically drops in this dynamic scenario: in fact, the error is larger than the one induced by the rigid model. This is explained by the fact that the dynamic model we consider is quite inaccurate: mostly, the antropometric model we use for the user only grossly approximates the real dynamics, as the user is free to move his torso in the exoskeleton. Just like in the static case, we believe these results can be largely improved by building a more accurate dynamic model. Extra difficulties are present however in the fact that we would need information about the complete motion of the user, and the fact that the support foot can tilt on the ground. Furthermore, in a real world scenario, this exoskeleton will be used by many users having different morphologies. A dynamics based estimator would be quite sensible to such parameters change, requiring a user-dependent model. On the contrary, because the motion of the exoskeleton does not drastically change with each user, the current kinematic based approach is insensitive to the load, and has already been tested on several users with very similar performance. In the results presented here, no modification of any kind was needed to go from an empty exoskeleton to an exoskeleton with a user. This is a strong argument in favor of dynamics-free observers, in the context of exoskeletons.

B. *Using the Estimator in Closed-Loop Control*

The aim of this estimator is to be used in closed-loop control, to compensate for the detrimental effect these deformations have on the positioning accuracy and the equilibrium of the system. Below, we present a simple control strategy tested in a quasi-static scenario.

Consider the exoskeleton in single support, in a static posture or following a quasi-static trajectory. Let ${}^{\mathcal{L}}M^*_{foot}$ be the target flying foot trajectory. Because of the deformations, even if one assumes perfect trajectory tracking on the motor side, the flying foot does not follow the correct trajectory. This is specifically noticeable when trying to land the foot on the ground: the impact happens much earlier than expected. In fact, if we generate a very slow stepping trajectory, which brings the flying foot from an airborne position to the ground, and play it on the robot to the end, the flexibilities cause the robot to strike the ground earlier than expected. If this is not taken into account, the robot continues to lower the foot after touchdown, and thus pushes on the ground: this destabilizes the robot and causes it to fall.

The correction we implement is based on inverse kinematics only. If there were no deformations, the position of the flying foot would be given by the encoders and the rigid model according to

$$ {}^{\mathcal{L}}M_{foot,r} = f_r(\boldsymbol{q}) \tag{23}$$

In that context, getting the flying foot to reach ${}^{\mathcal{L}}M^*_{foot}$ simply consists in solving an inverse kinematic problem. A well-known solution to this problem, which yields continuous joint position and velocity, consists in inverting the second derivative of (23): this is known as second-order inverse kinematics (the interested reader is referred at [24, Equation (4)], [25] and references therein). Here, we denote this algorithm IK. Given a trajectory for ${}^{\mathcal{L}}M_{foot,r}$, IK yields a joint trajectory such that the foot converges to the target trajectory. This control law thus writes

$$ \ddot{\boldsymbol{q}}^* = IK({}^{\mathcal{L}}M_{foot,r}) \tag{24}$$

In the presence of deformations, the estimator presented in this letter gives an estimate of the pose of the flying foot, ${}^{\mathcal{L}}\hat{M}_{foot}$. Then let us define $\hat{M}_d \triangleq {}^{\mathcal{L}}\hat{M}_{foot}\,{}^{\mathcal{L}}M^{-1}_{foot,r}$ the deformation homogeneous matrix: (23) is then modified into

$$ \hat{M}_d^{-1\,\mathcal{L}}M_{foot} = f_r(\boldsymbol{q}) \tag{25}$$

Thus, to track the trajectory ${}^{\mathcal{L}}M^*_{foot}$, we simply implement

$$ \ddot{\boldsymbol{q}}^* = IK(\hat{M}_d^{-1\,\mathcal{L}}M^*_{foot}) \tag{26}$$

Eq. (26) can be reinterpreted as follow: we subtract the estimated deformation from the trajectory before doing the inverse kinematics. To compute the second-order inverse kinematics in (26), it is required to know the first two derivatives of the reference trajectory, i.e. ${}^{\mathcal{L}}\boldsymbol{v}_{d/W}$ and ${}^{\mathcal{L}}\dot{\boldsymbol{v}}_{d/W}$. The first derivative, i.e. velocity, is directly available through the presented estimator, but an acceleration estimate is lacking. Since we are working in a quasi-static case, we here make the assumption that ${}^{\mathcal{L}}\dot{\boldsymbol{v}}_d \approx 0$: in other words, we neglect the dynamics of the flexibility. At a given time t, we compensate the deformation considering that our action has no impact on this deformation (i.e $\hat{M}_d$ is slowly varying). Certainly, this gross approximation would not be sufficient if we were trying to follow a fast trajectory, e.g. while walking.

In the quasi-static case however, the proposed control scheme is sufficient to get good results. Fig. 5 reports the comparison of two experiments, in which the left foot was asked to follow a slow stride trajectory bringing it to the ground. In the experiment presented on the left, the trajectory is played without any compensation (i.e. using (24)). This results in the foot being approximately 2 cm too low: it hits the ground early, at $t = 5$ s, and the impact causes the robot to fall. On the contrary, the presented control, (26), manages to bring the left foot much closer to its desired trajectory. The foot now impacts much later, and the robot no longer falls.

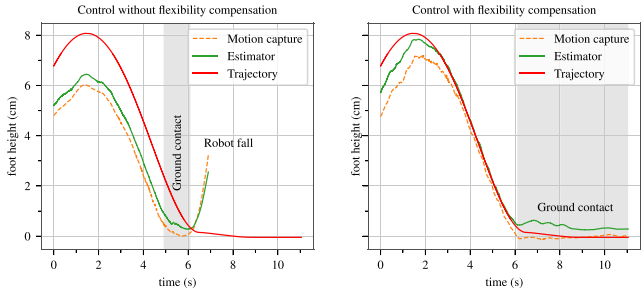

Fig. 5. Comparison of two experiments: tracking the same trajectory (in closed-loop) with (right) and without (left) flexibility compensation. The gray zone corresponds to the time during which the left foot force sensor measures ground contact.

This control has some weaknesses, due to the fact that we are neglecting the dynamics of the flexibility in (26): this is only true when doing slow motion, which limits the gains of the inverse kinematics algorithm in order to prevent oscillations. These low gains are the reason for the relatively slow convergence phase that can be observed at the beginning, or the remaining static error at the end (this error is created as the foot hits the ground, and is not compensated by the controller). Future work should focus on these weaknesses.

V. Conclusion

In this paper, we have presented a simple observation methodology for estimating the configuration of a legged robot with an arbitrary number of flexibilities. This estimator relies on a flat foot assumption and a flexible kinematic model, obtained by adding rotational degrees of freedom to the rigid kinematics, to model these flexibilities. This modeling approach enables us to break down the full state estimation problem into estimating n rotations with n IMUs, something that can be done using state-of-the-art estimators and a careful handling of the non-observable part. These estimations are then combined into the flexible model to give the corresponding position and velocity estimation.

This observation methodology has been tested experimentally on an exoskeleton, where it proves suitable for both the static and dynamic case, achieving a position accuracy of 1 cm in both cases, using low-cost IMUs. It also outperforms our previously designed dynamics-based EKF: in particular, the fact that it no longer requires difficult to identify parameters of the dynamics (such as inertia and stiffness) makes this approach robust and appealing for use in an exoskeleton, where the presence of a user introduces many uncertainties. This estimator was then used in closed-loop control to compensate for the effect of these deformations statically, using a geometric correction term. This controller was successfully tested on slow trajectories, and validates the performance of the estimator and its online use.

Future work include improving this control scheme in order to handle more rapid trajectory: this likely requires relaxing our hypothesis that ${}^{\mathcal{L}}\dot{\boldsymbol{v}}_d \approx 0$. The attitude estimation framework could also be improved, for instance by improving the hypothesis that the accelerometer measures only gravity by exploiting kinematic relationships between IMUs and encoders, in a manner similar to [15]. Finally, this methodology can be naturally extended to remove the flat ground hypothesis by adding IMUs in the robot feet to estimate the corresponding rotation using the same method, enabling walking on slanted or soft surfaces. This extension will be the subject of further investigations.

APPENDIX A
PROOF OF THEOREM 1

Let $R \in SO(3)$ be an arbitrary rotation matrix.
We define $\theta \triangleq |\alpha(\boldsymbol{t}(R),\ \boldsymbol{e}_z)|$ and

$$\mathcal{A} \triangleq \{P \in SO(3)\ \mid\ \boldsymbol{t}(P) = \boldsymbol{t}(R)\}$$

For any $P \in \mathcal{A}$, we define $R_z \triangleq RP^T$. Then as

$$\boldsymbol{t}(P) = \boldsymbol{t}(R) \iff P^T\boldsymbol{e}_z = R^T\boldsymbol{e}_z \iff \boldsymbol{e}_z = R_z^T\boldsymbol{e}_z$$

R_z is indeed a rotation of axis $\boldsymbol{e}_z$, yielding a decomposition of R according to (15). Thus, we only need to show that $\mathcal{A}$ has a unique minimum given by (17). Using (13) on $\boldsymbol{t}(R)$ yields

$$||P|| \geq |\alpha\left(\boldsymbol{t}(R),\ P\boldsymbol{t}(R)\right)| = |\alpha\left(\boldsymbol{t}(R),\ P\boldsymbol{t}(P)\right)| = \theta \quad (27)$$

If $R^T\boldsymbol{e}_z = -\boldsymbol{e}_z$, any rotation of angle π around a unit vector normal to $\boldsymbol{e}_z$ is a minimum over $\mathcal{A}$: thus the proposed decomposition exists but is not unique.

If $R^T\boldsymbol{e}_z = \boldsymbol{e}_z$, the identity matrix is trivially the only minimum over $\mathcal{A}$.

Finally, we consider the case where $R^T\boldsymbol{e}_z$ is not colinear to $\boldsymbol{e}_z$. Let R_s be an element of $\mathcal{A}$ of norm θ. We call $\boldsymbol{v}$ its axis of rotation, and use the property (demonstrated in [21]) that, for any nonzero vector $\boldsymbol{a}$,

$$|\alpha\left(\boldsymbol{a},\ R_s\boldsymbol{a}\right)| = ||R_s|| \iff \boldsymbol{a} \text{ is orthogonal to } \boldsymbol{v} \quad (28)$$

Consequently, as

$$|\alpha\left(\boldsymbol{t}(R_s),\ R_s\boldsymbol{t}(R_s)\right)| = |\alpha\left(R_s^T\boldsymbol{e}_z,\ \boldsymbol{e}_z\right)| = ||R_s|| \quad (29)$$

$$|\alpha\left(\boldsymbol{e}_z,\ R_s\boldsymbol{e}_z\right)| = |\alpha\left(R_s^T\boldsymbol{e}_z,\ \boldsymbol{e}_z\right)| = ||R_s|| \quad (30)$$

$\boldsymbol{v}$ is orthogonal to both $\boldsymbol{e}_z$ and $\boldsymbol{t}(R_s)$. As these vectors are not colinear, this means that $\boldsymbol{v} \in span(\boldsymbol{e}_z \times \boldsymbol{t}(R_s))$. Since $\boldsymbol{v}$ is a unit vector, there are only two possible choices

- $\boldsymbol{v}_1 = \frac{\boldsymbol{e}_z \times R^T\boldsymbol{e}_z}{||\boldsymbol{e}_z \times R^T\boldsymbol{e}_z||}$, in which case $R_s = \mathcal{R}(\boldsymbol{v}_1, \theta)$ to verify $R_s^T\boldsymbol{e}_z = \boldsymbol{t}(R)$.
- $\boldsymbol{v}_2 = -\frac{\boldsymbol{e}_z \times R^T\boldsymbol{e}_z}{||\boldsymbol{e}_z \times R^T\boldsymbol{e}_z||}$, in which case $R_s = \mathcal{R}(\boldsymbol{v}_2, -\theta)$ to verify $R_s^T\boldsymbol{e}_z = \boldsymbol{t}(R)$.

As $\boldsymbol{v}_2 = -\boldsymbol{v}_1$ and $\mathcal{R}(\boldsymbol{v}, \theta) = \mathcal{R}(-\boldsymbol{v}, -\theta)$, this analysis yields a unique candidate for the minimum, which is indeed the value given in (17). This ends the proof.

REFERENCES

[1] J. Grizzle, C. Chevallereau, R. Sinnet, and A. Ames, "Models, feedback control, and open problems of 3D bipedal robotic walking," *Automatica*, vol. 50, no. 8, pp. 1955–1988, Aug. 2014.

[2] C. Chevallereau, D. Djoudi, and J. W. Grizzle, "Stable bipedal walking with foot rotation through direct regulation of the zero moment point," *IEEE Trans. Robot.*, vol. 24, no. 2, pp. 390–401, Apr. 2008.

[3] M. Bloesch *et al.*, "State estimation for legged robots—consistent fusion of leg kinematics and IMU," *Robotics*, vol. 17, pp. 17–24, 2013.

[4] M. Fallon, M. Antone, N. Roy, and S. Teller, "Drift-free humanoid state estimation fusing kinematic, inertial and LIDAR sensing," in *Proc. IEEE-RAS Int. Conf. Humanoid Robots*, Nov. 2014, pp. 112–119.

[5] N. Rotella, M. Bloesch, L. Righetti, and S. Schaal, "State estimation for a humanoid robot," in *Proc. IEEE/RSJ Int. Conf. Intell. Robots Syst.*, pp. 952–958, Sep. 2014.

[6] R. Hartley, M. Jadidi, J. Grizzle, and R. Eustice, "Contact-aided invariant extended Kalman filtering for legged robot state estimation," in *Proc. Robot., Sci. Syst.*, May 2018.

[7] O. Harib *et al.*, "Feedback control of an exoskeleton for paraplegics: Toward robustly stable, hands-free dynamic walking," *IEEE Control Syst. Mag.*, vol. 38, no. 6, pp. 61–87, Dec. 2018.

[8] M. Benallegue and F. Lamiraux, "Estimation and stabilization of humanoid flexibility deformation using only inertial measurement units and contact information," *Int. J. Humanoid Robot.*, vol. 12, no. 3, Sep. 2015, Art. no. 1550025.

[9] T. Flayols, A. Del Prete, P. Wensing, A. Mifsud, M. Benallegue, and O. Stasse, "Experimental evaluation of simple estimators for humanoid robots," in *Proc. IEEE-RAS Int. Conf. Humanoid Robot.*, Nov. 2017, pp. 889–895.

[10] A. Mifsud, M. Benallegue, and F. Lamiraux, "Estimation of contact forces and floating base kinematics of a humanoid robot using only inertial measurement units," in *Proc. IEEE/RSJ Int. Conf. Intell. Robots Syst.*, Sep. 2015, pp. 3374–3379.

[11] V. Lebastard, Y. Aoustin, and F. Plestan, "Step-by-step sliding mode observer for control of a walking biped robot by using only actuated variables measurement," in *Proc. IEEE/RSJ Int. Conf. Intell. Robots Syst.*, Aug. 2005, pp. 559–564.

[12] J. Grizzle, J.-H. Choi, H. Hammouri, and B. Morris, "On observer-based feedback stabilization of periodic orbits in bipedal locomotion," *Methods Models Autom. Robot.*, 2007, pp. 27–30.

[13] M. Vigne, A. El Khoury, M. Masselin, F. D. Meglio, and N. Petit, "Estimation of multiple flexibilities of an articulated system using inertial measurements," in *Proc. IEEE Conf. Decis. Control*, Dec. 2018, pp. 6779–6785.

[14] R. Mahony, T. Hamel, and J. Pflimlin, "Nonlinear complementary filters on the special orthogonal group," *IEEE Trans. Autom. Control*, vol. 53, no. 5, pp. 1203–1217, Jun. 2008.

[15] M. Benallegue, A. Benallegue, and Y. Chitour, "Tilt estimator for 3D non-rigid pendulum based on a tri-axial accelerometer and gyrometer," in *Proc. IEEE-RAS Int. Conf. Humanoid Robot.*, Nov. 2017, pp. 830–835.

[16] J. Crassidis, L. Markley, and Y. Cheng, "Survey of nonlinear attitude estimation methods," *J. Guid., Control, Dyn.*, vol. 30, no. 1, pp. 12–28, 2007.

[17] R. Featherstone, *Rigid Body Dynamics Algorithms*. Boston, MA, USA: Springer, 2008.

[18] J. Carpentier *et al.*, "The Pinocchio C++ library: A fast and flexible implementation of rigid body dynamics algorithms and their analytical derivatives," in *Proc. Int. Symp. Syst. Integrations*, Jan. 2019, pp. 614–619.

[19] P. Martin and I. Sarras, "Partial attitude estimation from a single measurement vector," in *Proc. 2nd IEEE Conf. Control Technol. Appl.*, 2018, pp. 1325–1331.

[20] P. Baerlocher and R. Boulic, "Parametrization and range of motion of the ball-and-socket joint," in *Deformable Avatars: IFIP TC5/WG5.10 DEFORM'2000 Workshop November 29–30, 2000 Geneva, Switzerland*, Boston, MA, USA: Springer, 2001, pp. 180–190.

[21] D. Huynh, "Metrics for 3D rotations: Comparison and analysis," *J. Math. Imag. Vision*, vol. 35, no. 2, pp. 155–164, Oct. 2009.

[22] M. Vigne, A. El Khoury, F. D. Meglio, and N. Petit, "Video of the experiments on Atalante." 2019. Online. Available: https://youtu.be/Jw5jVPWjyqE

[23] D. A. Winter, *Biomechanics and Motor Control of Human Movement*. Hoboken, NJ, USA: Wiley, 2009.

[24] F. Caccavale, S. Chiaverini, and B. Siciliano, "Second-order kinematic control of robot manipulators with Jacobian damped least-squares inverse: theory and experiments," *IEEE/ASME Trans. Mechatronics*, vol. 2, no. 3, pp. 188–194, Sep. 1997.

[25] M. W. Spong, *Robot Dynamics and Control*. 1st ed. New York, NY, USA: Wiley, 1989.